



Cite this: *RSC Adv.*, 2022, 12, 17905

Nanomagnetic macrocyclic Schiff-base–Mn(II) complex: an efficient heterogeneous catalyst for click approach synthesis of novel β -substituted-1,2,3-triazoles†

Saade Abdalkareem Jasim,^a Yassine Riadi,^b  ^{*b} Hasan Sh. Majdi^c and Usama S. Altimari^d

In the present work, a novel symmetrical 15-membered macrocyclic Schiff base complex of manganese was prepared using the reaction of the synthetic 2,6-diacetylpyridine functionalized Fe_3O_4 MNPs with 2,2-(piperazine-1,4-diyl)dianiline and Mn(II) bromide salt *via* a template approach. The resulting $[\text{Fe}_3\text{O}_4@\text{PAM-Schiff-base-Mn}][\text{ClO}_4]$ heterogenized complex was characterized using FT-IR, XRD, BET, TGA, EDX, X-ray-mapping, SEM, TEM and VSM analysis. To demonstrate proof of concept, Huisgen 1,3-dipolar cycloaddition synthesis of 1,2,3-triazoles was selected to evaluate the activity and reusability of the catalyst. The ethanol as a green solvent proved to be an excellent reaction medium for this synthesis. Yields of up to 100% were obtained in some cases. Significantly, as demonstrated, $[\text{Fe}_3\text{O}_4@\text{PAM-Schiff-base-Mn}][\text{ClO}_4]$ catalyst was recycled for 8 cycles without losing catalytic activity under the optimized reaction conditions. The hot filtration and ICP-OES tests ratified that there was no leaching of metal during the catalytic reaction, indicating the heterogeneous manner of the catalyst.

Received 23rd April 2022
Accepted 3rd June 2022

DOI: 10.1039/d2ra02587f

rsc.li/rsc-advances

1. Introduction

A multicomponent approach is associated with employing more than two different substrates in order to generate the most important heterocyclic molecules.^{1–5} These techniques result in generating the targeted products in green and safer manners and cause an acceleration in the reaction rates assisting the reaction completion in shorter times under milder conditions with high yields.^{6–10} These factors make the multicomponent approach more convenient, time efficient, simple and easily controlled as compared to conventional methods.^{11–15} Therefore, this unique technique can be utilized for a green, economical and environmentally-friendly approach for both the synthesis and application of the engineered nanocatalysts.^{1,5,16,17} This is owing to the fact that the rationally synthesized nanocatalysts are designed to have enhanced

catalytic activity and selectivity towards chemical processes under study.¹⁸

Among various heterocyclic molecules, N-containing heterocycles are considered as the main class of drugs.^{17,19–23} In this sense, triazoles compounds, as chemical intermediates, are broadly utilized in numerous industrial formulations including biological and pharmaceutical ones.^{24,25} Towards this end, various approaches have been utilized to synthesize 1,2,3-triazole moieties.^{26–28} Moreover, the catalytic Huisgen 1,3-dipolar cycloaddition of epoxides, thiiranes and aziridines with NaN_3 and terminal alkynes generated the corresponding 1,2,3-triazoles, considered as one of the most relevant methods.^{29–32} The obtained triazoles are precious intermediates in preparing several combinations containing, antioxidants, pharmaceuticals, drugs, agrochemicals, dyes, pesticides and polymers.^{33–36}

Green chemistry seeks to find novel chemical methods for synthesis of the targeted products while decreasing the pollutants that are formed as the by-product during the synthesis process.^{37–42} Moreover, the main purpose of green chemistry is to achieve benign-by-design materials for a more sustainable future.^{43–45} Along these lines, designing and finding stable and highly active catalysts are considered as two main targets of the green chemistry objectives.^{46–50} Recently, there has been an outstanding attention to chemical processes involving heterogeneous catalysts with extraordinary activity, high surface area to volume and good recyclability.^{51,52} Heterogenized catalytic complexes are new organic–inorganic hybrid compounds

^aMedical Laboratory Techniques Department, Al-Maarif University College, Al-Anbar-Ramadi, Iraq

^bDepartment of Pharmaceutics, College of Pharmacy, Prince Sattam Bin Abdulaziz University, Al-Kharj, 11942, Saudi Arabia. E-mail: yassine.riadi2022@gmail.com; y.riadi2@psau.edu.sa

^cDepartment Chemical Engineering and Petroleum Industries, Al-Mustaqbal University College, 51001, Iraq

^dDepartment of Pharmaceutics, Al-Nisour University College, Baghdad, Iraq

† Electronic supplementary information (ESI) available. See <https://doi.org/10.1039/d2ra02587f>


prepared from metallic ions and organic linkers, bonded to the surface of inorganic insoluble nanomaterials.^{53–55}

Majority of the nanocatalysts reported in literature are derived from nanoparticles in either metallic, metal oxides or organic forms.^{56–59} Amongst these, magnetic nanoparticles have been of major interest to researchers in area of catalysis owing to the ability to heterogenize the nanoparticles and provide ease of catalyst separation *via* magnetic decantation.^{60–62} Significantly, the magnetic nanoparticles, specifically iron oxide nanoparticles, have been widely explored due to their unique features containing high special surface area, structural variability and excellent thermal stability.^{63–65} These materials have been widely employed in diverse fields.^{66–68} They have also emerged as efficient heterogeneous catalytic supports because they can easily bond to several organic linkers and provide higher activity, stability and surface area as compared to homogeneous catalysts.^{34,69–71}

Both the salen and salamo-based ligands are important classes of organic ligands which have attracted considerable attention owing to their N₂O₂-donor structure and organometallic properties such as high excellent coordination ability to transition metal ions.^{72–74}

Nanoparticles based on Schiff's bases-metal complexes are important classes of hetrogenized organic ligands and complexes and important parts of green chemistry, they constitute the largest and the most diverse family of organic ligands with chemical, biomedical and industrial significance.^{75–77} In these complexes, both of the nitrogen and carbon centers are coordinate to metal ions *via* electron donation from C=N π and σ^* orbitals into the empty orbital of transition metals and electron donation from the transition metal d orbital into the C=N π^* orbital (π -back bonding) respectively.^{78–80} These compounds are privileged in the structure of many transition metal complexes, catalysts, drugs and biological and pharmaceutical molecules.^{81–84} Therefore, the development of novel and ecofriendly catalytic systems based on the Schiff-base ligands is an important challenge in organic and inorganic synthesis.

In this work, our main goal was to synthesize and characterize a novel Fe₃O₄ immobilized 15-membered-ring symmetrical pentaaza macrocyclic Schiff base complex of manganese (II) using a simple approach and the targeted heterogeneous catalytic Mn(II) complex as the catalyst for the synthesis of the biologically active β -thiolo/benzyl-1,2,3-triazoles.

2. Experimental

2.1. Materials

All commercially available reagents and solvents were used without further purification and were obtained from Sigma-Aldrich. The synthesis of β -substituted-1,2,3-triazoles were carried out in a 15 mL pressurized vial.

2.2. Instrumental measurements

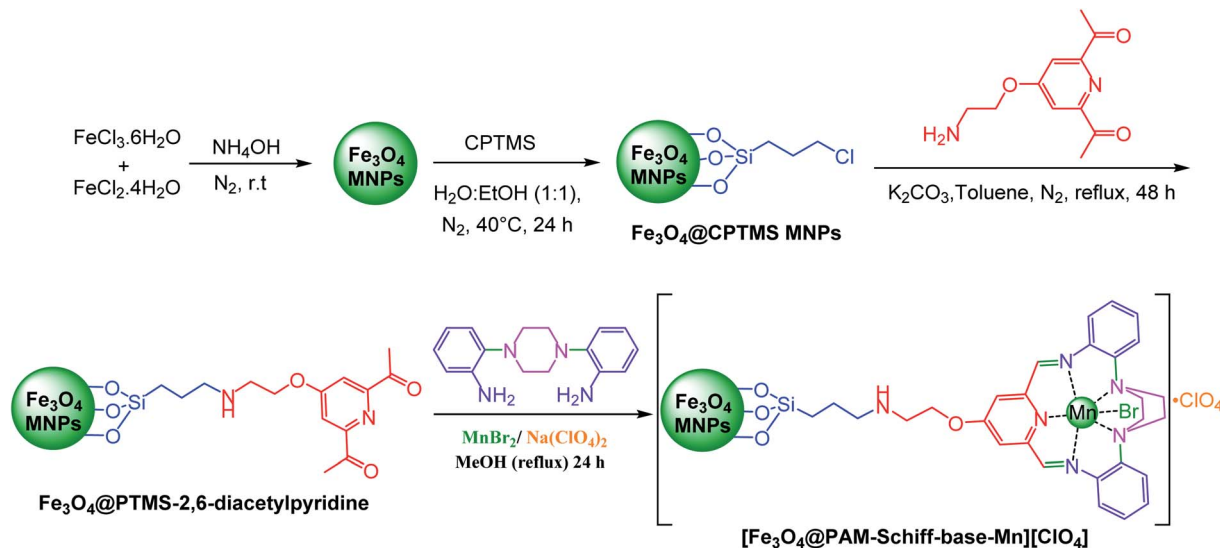
Liquid phase ¹H and ¹³C NMR spectra were recorded on a Bruker Avance III 400 MHz, and Bruker Avance III 101 MHz

spectrometers. NMR spectra were processed using MestreNova version 6.0.2-5475 software. Fourier-transform infrared (FT-IR) spectra were obtained on an Agilent Cary 630 FTIR benchtop spectrometer with a range from 4000 to 500 cm⁻¹. X-Ray diffraction (XRD) patterns were acquired from 10° to 80° for the 2 θ angles at room temperature with a Shimadzu XRD7000 using Cu K- α radiation with λ = 1.54184 nm, operating at 40 kV and 30 mA and scan speed of 2 °C min⁻¹. Nitrogen physisorption measurements were performed at 77 K by using a NOVA 4200e model from Quantachrome. Samples were degassed and dried for 4 h at 90 °C under vacuum before analysis. Surface areas were calculated according to the BET equation, whereas the average pore diameter and pore volume were obtained from the N₂ desorption branch. Thermogravimetric analysis (TGA) was performed under air atmosphere using a TA Instruments TGA 2050 thermogravimetric analyser, a typical sample of 10 mg was used. The spectra were recorded from 25 °C to 800 °C using a heating rate of 10 °C min⁻¹. Quantitative inductively coupled plasma-optical emission spectrometry (ICP-OES) was performed using a SPECTRO ARCOS ICP-OES analyser. Scanning electron microscopy (SEM) analysis were performed with a Quanta 250 field emission scanning electron microscope (FEI Co., USA), equipped with an Oxford X-MAX50 energy dispersive spectrometer (EDS) (Oxford, UK). Transmission electron microscope (TEM) analysis were performed with a 200 kV JEOL (Tokyo, Japan). Value stream mapping (VSM) analysis was carried out using a vibrating sample magnetometer (VSM, LakeShore VSM 7400).

2.3. Typical procedure for the preparation of [Fe₃O₄@PAM-Schiff-base-Mn][ClO₄] complex

Synthesis of iron oxide nanoparticles was carried out in aqueous solution by coprecipitation of ferric ions with 25% ammonium hydroxide solution, followed by capping of the as-prepared nanosized Fe₃O₄ nanoparticles with (3-chloropropyl)trimethoxysilane linker according to a protocol reported by Barikani *et al.*⁸⁵ Afterwards, 5 mmol of 4-(2-aminoethoxy)-2,6-diacetylpyridine moiety was immobilized on 2 g of Fe₃O₄@CPTMS MNPs *via* nucleophilic substitution reaction in 100 mL of toluene. To this solution, 5 mmol of K₂CO₃ was added and the reaction was stirred for 48 h at reflux conditions. Next, the reaction mixture was separated using magnetic decantation and, then, washed thrice with absolute ethanol. The obtained product was then dried in vacuum oven. Afterwards, Fe₃O₄@PTMS-2,6-diacetylpyridine (2 g) was dispersed in (150 mL) of methanol and, then, 5 mmol Mn(II) bromide salt and 2,2-(piperazine-1,4-diyl)dianiline (5 mmol) were dissolved in (50 mL) methanol and dropwise added into the mixture. Later, the reaction mixture was stirred for 24 hours at reflux conditions. Subsequently, 3 mmol of sodium perchlorate was added to the mixture and, then, refluxed for 8 h. In addition, the acquired solid was magnetically isolated from the mixture, rinsed multiple times with methanol (50 mL), dichloromethane (50 mL) and acetone (50 mL) and, finally, dried for 12 hours at 80 °C under vacuum. Furthermore, [Fe₃O₄@PAM-Schiff-base-Mn][ClO₄] MNPs and its intermediates were characterized using various analytical techniques (Scheme 1).



Scheme 1 Stepwise synthesis of $[\text{Fe}_3\text{O}_4\text{@PAM-Schiff base-Mn}][\text{ClO}_4]$.

2.4. General procedure for the preparation of 1,2,3-triazoles products catalyzed by $[\text{Fe}_3\text{O}_4\text{@PAM-Schiff base-Mn}][\text{ClO}_4]$ complex

The catalytic endeavor of $[\text{Fe}_3\text{O}_4\text{@PAM-Schiff base-Mn}][\text{ClO}_4]$ heterogeneous complex was indicated in one of the click reactions (Huisgen 1,3-dipolar cycloaddition). In this reaction, a mixture of terminal alkyne (1 mmol), substituted epoxides or thiiranes (1 mmol), NaN_3 (1.3 eq.) and $[\text{Fe}_3\text{O}_4\text{@PAM-Schiff base-Mn}][\text{ClO}_4]$ nanocatalyst (12 mg) was added to the reaction in ethanol (10 mL) and, then, refluxed for appropriate times. After completion of the reaction (monitored by TLC), the catalyst was separated through the magnetic decantation and, then, washed several times with ethanol. Afterwards, the solvent was evaporated. Moreover, the obtained solid was extracted with 3×20 mL water and ethyl acetate and, then, dried over anhydrous sodium sulphate filtered to give the corresponding product. The products were purified by recrystallization in $\text{EtOH}/\text{H}_2\text{O}$ (1 : 1) to give the pure 1,2,3-triazoles and, then, characterized using NMR spectroscopy. (See ESI†).

3. Results and discussion

3.1. Characterization of the catalyst

Preparation of the catalyst is shown in Scheme 1. The obtained catalyst was thoroughly characterized using the following techniques.

3.1.1. FT-IR spectroscopy. Furthermore, we investigated the as-prepared nanomaterials by FTIR analysis, as shown in Fig. 1. We can determine the synthesis and robust interaction of linker and ligand with the support. Fig. 1 represents the comparative FTIR spectra of (a) Fe_3O_4 , (b) $\text{Fe}_3\text{O}_4\text{@CPTMS}$, (c) $\text{Fe}_3\text{O}_4\text{@PTMS-2,6-diacetylpyridine}$ and (d) $[\text{Fe}_3\text{O}_4\text{@PAM-Schiff base-Mn}][\text{ClO}_4]$. The Fe_3O_4 and $\text{Fe}_3\text{O}_4\text{@CPTMS}$ FT-IR results are exactly consistent with the previous reports.^{86,87} In the case of $\text{Fe}_3\text{O}_4\text{@PTMS-2,6-diacetylpyridine}$, the absorption band of ($-\text{NH}$) appeared as a singlet peak at 3694 cm^{-1} from the 2,6-

diacetylpyridine moiety and C-Cl peak disappeared. Moreover, the absorption band at 1726 cm^{-1} is related to the acetyl $\text{C}=\text{O}$ groups, and absorption bands at $1550\text{--}1650\text{ cm}^{-1}$ are related to the aromatic $\text{C}=\text{C}$ bonds. The FT-IR of the synthesized $[\text{Fe}_3\text{O}_4\text{@PAM-Schiff base-Mn}][\text{ClO}_4]$ shows new absorption bands at $1590\text{--}1615\text{ cm}^{-1}$ which are related to the $\text{C}=\text{N}$ bonds confirming the generation of Mn-coordinated Schiff base complex.⁸⁸

3.1.2. XRD analysis. The resultant products was characterized using various techniques, *i.e.* powder X-ray diffraction (PXRD) spectra analyzed using $\text{Cu K}\alpha$ radiation 1.54 \AA . Fig. 2 shows the normal angle XRD pattern of the synthesized (a) Fe_3O_4 and (b) $[\text{Fe}_3\text{O}_4\text{@PAM-Schiff base-Mn}][\text{ClO}_4]$ with 2θ in the range of $10\text{--}80^\circ$. X-ray diffraction pattern reveals that Fe_3O_4 and $[\text{Fe}_3\text{O}_4\text{@PAM-Schiff base-Mn}][\text{ClO}_4]$ were found to be crystalline and exactly consistent with the previous reports for Fe_3O_4 MNPs. The results show that the $[\text{PAM-Schiff base-Mn}][\text{ClO}_4]$ complex, mounted on the surface of the Fe_3O_4 MNPs, would decrease the crystallinity in Fe_3O_4 due to addition of CPTMS on its surface containing the amorphous silica. However, the phase and structure were not destroyed after the chemical functionalization. Moreover, the presence of a broad peak at $2\theta = 20\text{--}27^\circ$ which is due to the amorphous silicon layer, demonstrating that the Fe_3O_4 structure was functionalized by CPTMS linker.^{26,27} In addition, after anchoring the $[\text{PAM-Schiff base-Mn}][\text{ClO}_4]$ complex, the new diffraction peaks were appeared at $2\theta = 32\text{--}35$; $40\text{--}42$ and $59\text{--}61^\circ$, that are related to a separate phase of Mn species in $[\text{Fe}_3\text{O}_4\text{@PAM-Schiff base-Mn}][\text{ClO}_4]$, confirming the complexation of Mn and its strong attachment over $\text{Fe}_3\text{O}_4\text{@PAM-Schiff base-Mn}$ composite.^{89,90} Finally, based on the Scherrer ($D = K\lambda/(\beta \cos \theta)$) equation, the average crystallite size of $[\text{Fe}_3\text{O}_4\text{@PAM-Schiff base-Mn}][\text{ClO}_4]$ nanoparticles was found to be about 17.42 nm .

3.1.3. BET analysis. Surface area and porosity were determined by Brunauer-Emmett-Teller using nitrogen gas for adsorption-desorption analysis at 77 K (Fig. 3). BET analysis



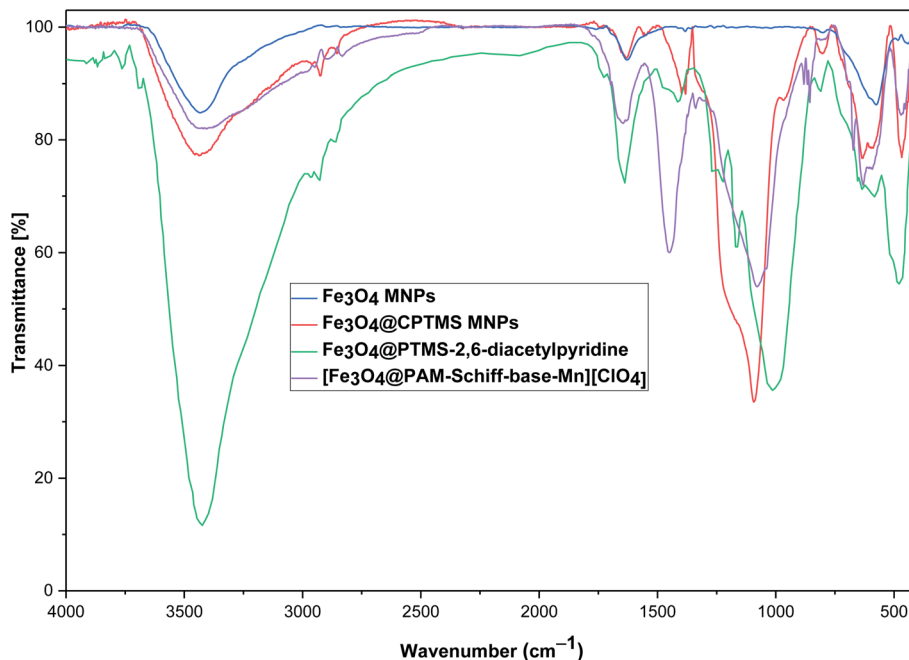


Fig. 1 FTIR of (a) Fe_3O_4 , (b) $\text{Fe}_3\text{O}_4\text{@CPTMS}$, (c) $\text{Fe}_3\text{O}_4\text{@PTMS-2,6-diacetylpyridine}$ and (d) $[\text{Fe}_3\text{O}_4\text{@PAM-Schiff base-Mn}][\text{ClO}_4]$ MNPs.

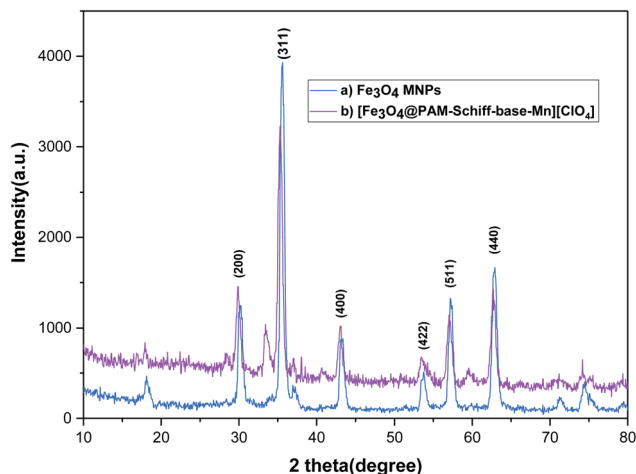


Fig. 2 XRD patterns of (a) Fe_3O_4 and (b) $[\text{Fe}_3\text{O}_4\text{@PAM-Schiff base-Mn}][\text{ClO}_4]$ MNPs.

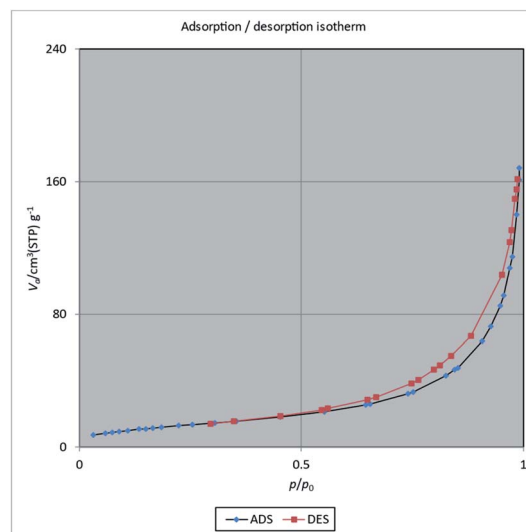


Fig. 3 N_2 adsorption-desorption isotherms of $[\text{Fe}_3\text{O}_4\text{@PAM-Schiff base-Mn}][\text{ClO}_4]$ MNPs.

gave the surface area of $[\text{Fe}_3\text{O}_4\text{@PAM-Schiff base-Mn}][\text{ClO}_4]$ to be about $81 \text{ m}^2 \text{ g}^{-1}$. Moreover, the pore volume and pore radius were determined as $0.2592 \text{ cm}^3 \text{ g}^{-1}$, 20.247 nm using BJH (Barret-Joyner-Halenda) analysis. It was also found out that, after loading the Mn complex on the support surface, there was a decrease in surface area of the parent Fe_3O_4 MNPs as compared to previous reports,⁹¹ that might be due to the loading of Mn catalytic complex happening on the surface of support.

3.1.4. TGA analysis. Thermogravimetric analysis determines the thermal stability of the synthesized (a) Fe_3O_4 , (b) $\text{Fe}_3\text{O}_4\text{@CPTMS}$, (c) $\text{Fe}_3\text{O}_4\text{@PTMS-2,6-diacetylpyridine}$ and (d) $[\text{Fe}_3\text{O}_4\text{@PAM-Schiff base-Mn}][\text{ClO}_4]$ MNPs (Fig. 4). The TGA

curves show that Fe_3O_4 and $\text{Fe}_3\text{O}_4\text{@CPTMS}$ are stable in a temperature range from room temperature to 200°C since $\text{Fe}_3\text{O}_4\text{@CPTMS}$ shows sudden and maximum weight loss of 7.5% from 300°C to 420°C that was the result of oxidative decomposition of the CPTMS organic functionalities by the elimination during pyrolysis process. In the case of $\text{Fe}_3\text{O}_4\text{@PTMS-2,6-diacetylpyridine}$ and $[\text{Fe}_3\text{O}_4\text{@PAM-Schiff base-Mn}][\text{ClO}_4]$ MNPs, the TGA curves show the mild mass loss occurring in below 200°C , initially attributed to the presence of moisture.⁹² The next mass loss corresponding to 11% and 17.5% up to 450°C was the result of oxidative decomposition of the



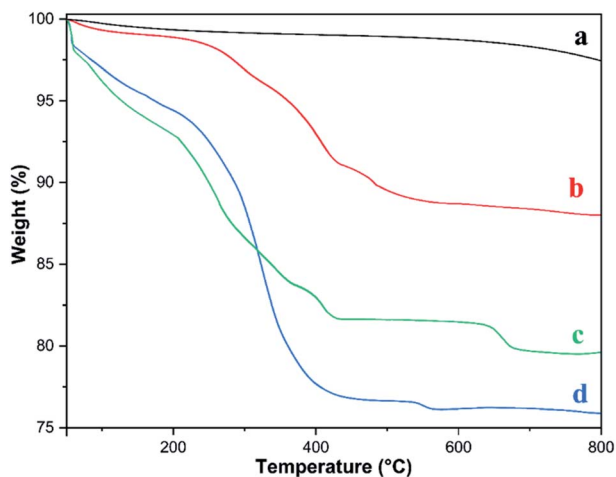


Fig. 4 TGA analysis of (a) Fe_3O_4 , (b) $\text{Fe}_3\text{O}_4\text{@CPTMS}$, (c) $\text{Fe}_3\text{O}_4\text{@PTMS-2,6-diacetylpyridine}$ and (d) $[\text{Fe}_3\text{O}_4\text{@PAM-Schiff base-Mn}][\text{ClO}_4]$ MNPs.

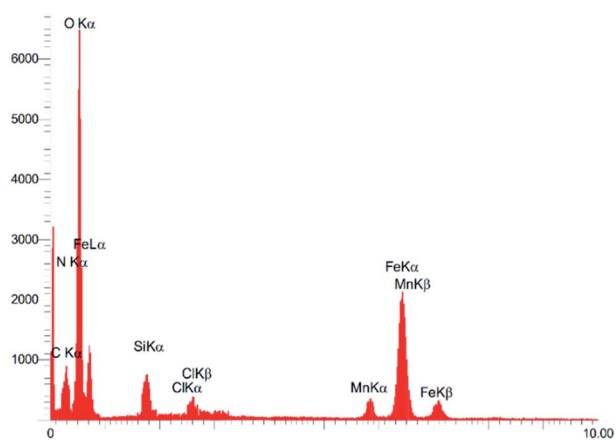


Fig. 5 EDX analysis of $[\text{Fe}_3\text{O}_4\text{@PAM-Schiff base-Mn}][\text{ClO}_4]$ MNPs.

PTMS-2,6-diacetylpyridine and $[\text{PAM-Schiff base-Mn}][\text{ClO}_4]$ organic groups, respectively, confirming the chemisorption of organic and organometallic layers on the Fe_3O_4 MNPs. All of these findings confirm the successful synthesis of $[\text{Fe}_3\text{O}_4\text{@PAM-Schiff base-Mn}][\text{ClO}_4]$.

3.1.5. EDX analysis. Subsequently, EDS analysis gives information about what elements are there with their percentage, as shown in Fig. 5. Additionally, EDS which is quantitative as well as qualitative analysis was used to evaluation of loading of $[\text{PAM-Schiff base-Mn}][\text{ClO}_4]$ complex on Fe_3O_4 . This analysis confirms the presence of Fe, O, Si, C, N Mn and Cl elements in the composition of $[\text{Fe}_3\text{O}_4\text{@PAM-Schiff base-Mn}][\text{ClO}_4]$. Furthermore, the ICP-OES analysis gave the idea of how much Mn is present. ICP-OES shows that there is $1.5 \times 10^{-3} \text{ mol g}^{-1}$ of Mn loaded on Schiff base functionalized magnetic nanoparticles.

3.1.6. X-ray-mapping analysis. The EDX mapping process is a standard procedure in order to identify and quantify the elemental composition of micron-sized samples of $[\text{Fe}_3\text{O}_4\text{@PAM-Schiff base-Mn}][\text{ClO}_4]$ – which are Fe, O, Si, C, N, Mn and Cl – as shown in Fig. 6.

3.1.7. SEM analysis. In order to find out the morphology and elemental composition of $[\text{Fe}_3\text{O}_4\text{@PAM-Schiff base-Mn}][\text{ClO}_4]$, the FE-SEM analysis was carried out (Fig. 7). It shows that $[\text{Fe}_3\text{O}_4\text{@PAM-Schiff base-Mn}][\text{ClO}_4]$ is made of quasi-uniform crystallites of spherical nanoparticles which are smooth and are seen in the agglomerated form in the image as shown in Fig. 7. The mean diameter of $[\text{Fe}_3\text{O}_4\text{@PAM-Schiff base-Mn}][\text{ClO}_4]$ was found out to be in the range of 70–93 nm.

3.1.8. TEM analysis. The $[\text{Fe}_3\text{O}_4\text{@PAM-Schiff base-Mn}][\text{ClO}_4]$ formation and evidence were investigated using TEM analysis (Fig. 8). The TEM micrographs further support the spherical shape with some nanoparticle aggregation morphology and occurrence of the minor dark spots of loaded Mn on $\text{Fe}_3\text{O}_4\text{@PAM-Schiff base-Mn}$ MNPs. Regarding the TEM, it is indicated that $[\text{Fe}_3\text{O}_4\text{@PAM-Schiff base-Mn}][\text{ClO}_4]$ consists of

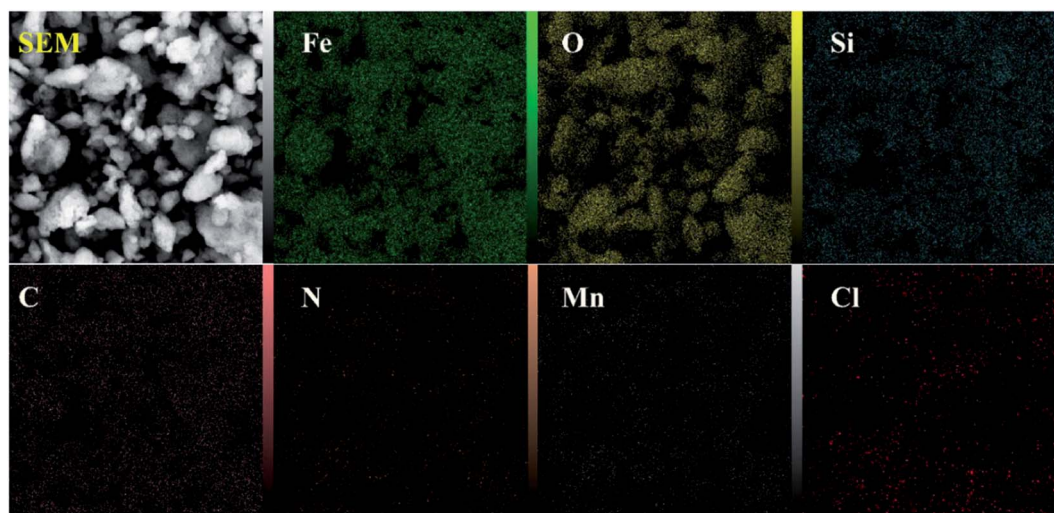


Fig. 6 EDX mapping images of $[\text{Fe}_3\text{O}_4\text{@PAM-Schiff base-Mn}][\text{ClO}_4]$ MNPs.

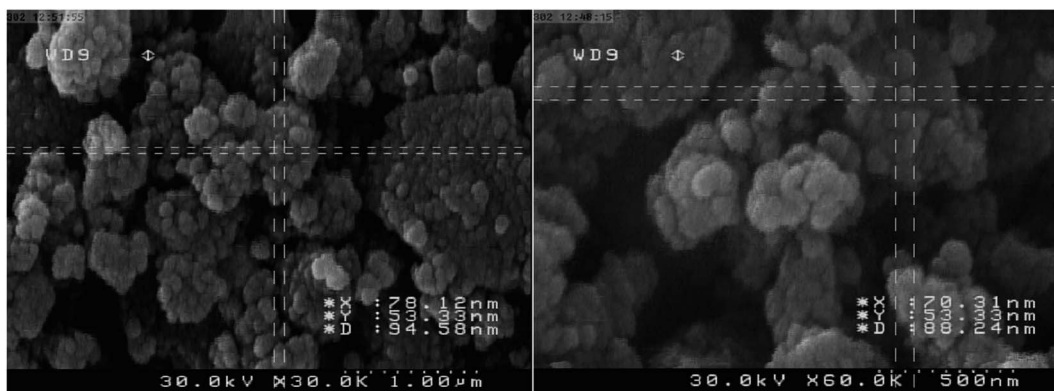


Fig. 7 SEM images of $[\text{Fe}_3\text{O}_4@\text{PAM-Schiff base-Mn}][\text{ClO}_4]$ MNPs.

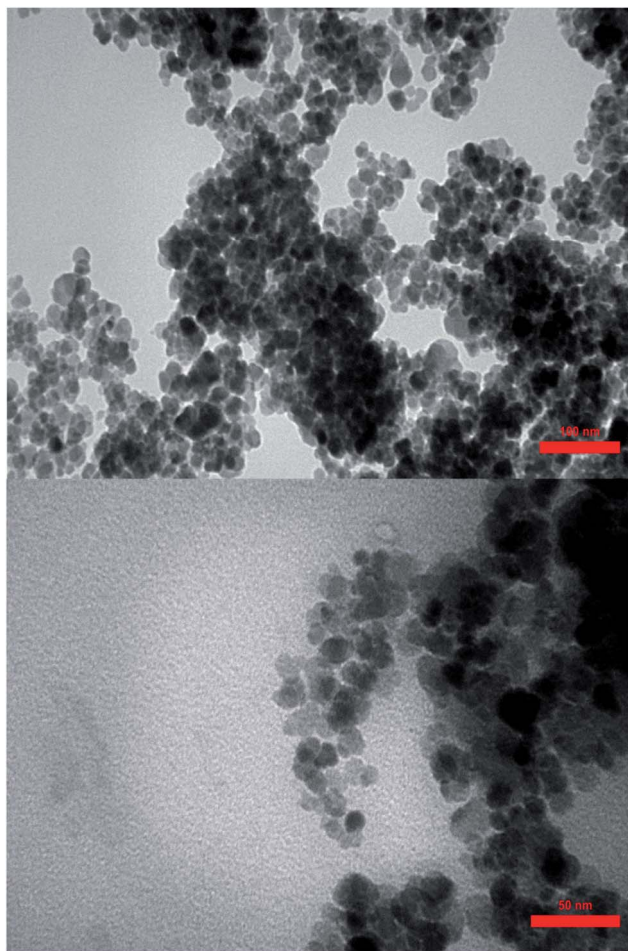


Fig. 8 TEM images of $[\text{Fe}_3\text{O}_4@\text{PAM-Schiff base-Mn}][\text{ClO}_4]$ MNPs.

a thin shell over the Fe_3O_4 core. The prepared nanoparticles reveal an average particle size, ranging from 21 to 28 nm.

3.1.9. VSM analysis. The evaluation of the magnetic properties of (a) Fe_3O_4 , (b) $\text{Fe}_3\text{O}_4@\text{CPTMS}$, (c) $\text{Fe}_3\text{O}_4@\text{PTMS-2,6-diacetylpyridine}$ and (d) $[\text{Fe}_3\text{O}_4@\text{PAM-Schiff base-Mn}][\text{ClO}_4]$ nanocomposites was performed by carrying out vibrating sample magnetometer (VSM) measurements. The magnetic

hysteresis curves of a-dc samples are shown in Fig. 9. The magnetization values for (a)–(d) samples were calculated as 78.29, 68.02, 53.11 and 45.27 emu g^{-1} , respectively. Thus, the superparamagnetic properties of Fe_3O_4 extremely reduced because of the attendance of the covered CPTMS shell and $[\text{@PAM-Schiff base-Mn}][\text{ClO}_4]$ catalytic species on its surface. Nevertheless, the $[\text{@PAM-Schiff base-Mn}][\text{ClO}_4]$ nanocatalyst is also evident from an easy separation using an external magnet.

3.2. Catalytic properties of magnetic system

After successful preparation and characterization of $[\text{Fe}_3\text{O}_4@\text{PAM-Schiff base-Mn}][\text{ClO}_4]$, its catalytic efficiency was examined for the Huisgen 1,3-dipolar cycloaddition reaction. This selection was based on the assumption that Mn catalyst seems to provide a potent weapon to cycloaddition of any substituted three-membered heterocycle (epoxide, thiirane and aziridine) with sodium azide and terminal alkynes.

3.2.1. Optimization of reaction conditions. During an effort to have Huisgen 1,3-dipolar cycloaddition reaction, the

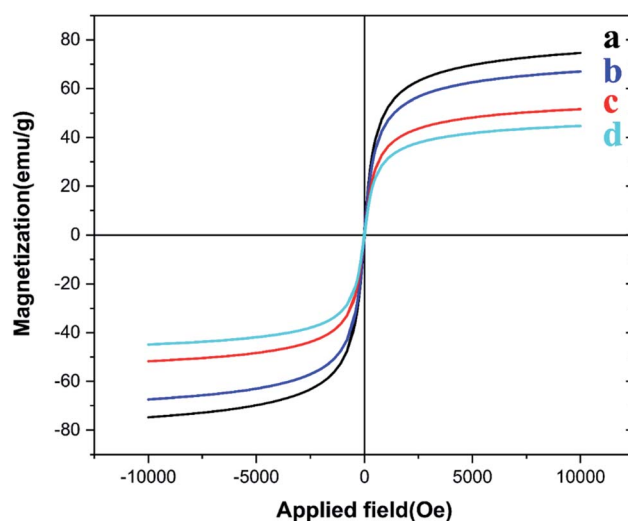
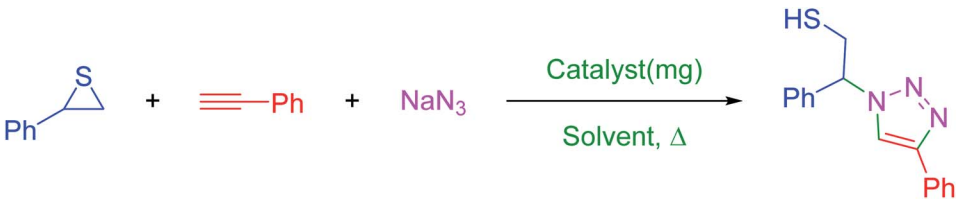


Fig. 9 VSM analysis of (a) Fe_3O_4 , (b) $\text{Fe}_3\text{O}_4@\text{CPTMS}$, (c) $\text{Fe}_3\text{O}_4@\text{PTMS-2,6-diacetylpyridine}$ and (d) $[\text{Fe}_3\text{O}_4@\text{PAM-Schiff base-Mn}][\text{ClO}_4]$ MNPs.



Table 1 Reaction of styrene episulfide with phenylacetylene and sodium azide catalysed by $\text{Fe}_3\text{O}_4@\text{SiO}_2\text{-PMA-Cu}$ under different conditions


Entry	Amount of catalyst (mg)	Solvent	Temperature (°C)	Time (min)	Yield ^{ab} (%)
1	—	EtOH	Reflux	10	0
2	2	EtOH	Reflux	15	43
3	3	EtOH	Reflux	15	75
4	5	EtOH	Reflux	15	81
5	8	EtOH	Reflux	15	94
6	10	EtOH	Reflux	15	98
7	12	EtOH	Reflux	15	100
8	15	EtOH	Reflux	15	100
9	12	MeOH	Reflux	15	95
10	12	H ₂ O	80	15	93
11	12	CH ₃ CN	Reflux	15	81
12	12	DMF	80	15	67
13	12	EtOAc	Reflux	15	73
14	12	THF	Reflux	15	Trace
15	12	<i>n</i> -Hexane	Reflux	15	28
16	12	CCl ₄	Reflux	15	17
17	12	Solvent free	80	15	Trace
18	12	EtOH	25	15	Trace
19	12	EtOH	40	15	57
20	12	EtOH	60	15	76
21	12	EtOH	65	15	84
22	12	EtOH	70	15	93

^a Reaction conditions: phenylacetylene (1 mmol), episulfide (1 mmol) and sodium azide (1.3 mmol) catalyst (mg) and solvent (10 mL). ^b Isolated yields.

reaction of phenyl acetylene, styrene episulfide and sodium azide in the presence of $[\text{Fe}_3\text{O}_4@\text{PAM-Schiff base-Mn}][\text{ClO}_4]$ as catalyst in ethanol (10 mL) was considered as the model reaction to optimize different reaction conditions. The observational findings are tabulated in Table 1.

3.2.1.1. Effect of catalyst content. Initially, the reaction was carried out using a varied catalyst amount in ethanol under reflux. The outcomes of the study are shown in Table 1. The reaction started with 2 mg of catalyst which gave 43% of the product and, then, the amount of the catalyst further increased to 12 mg as shown in Table 1, entries 2–6. It was found out that when there was 12 mg of the catalyst, the obtained yield was 100%. After increasing the catalyst amount to 15 mg, there was no significant difference in reaction time (Table 1, entry 8). Consequently, 12 mg of $[\text{Fe}_3\text{O}_4@\text{PAM-Schiff base-Mn}][\text{ClO}_4]$ was picked for further studies. The reaction was also performed without a catalyst and, accordingly, the productivity was very little as compared to the presence of the catalyst, which means that the catalyst performs a very important role in the reaction to enhance the isolated product (Table 1, entry 1).

3.2.1.2. Effect of solvent. It is well known that solvents have profound effects on the reaction progress and, hence, to make sure that EtOH is the most suitable solvent in conducting the reaction, in further studies, the model reaction was carried out under a variegated range of solvents from polar as well as non-polar and protic to aprotic (Table 1). In the case of non-polar solvents, the low solubility of reactants proceeds the reaction with a lower rate and efficiency. Moreover, the reaction did not proceed to any extent without solvent (Table 1, entry 17). As well the polar protic solvents, like ethanol, methanol and water with dissociable hydrogen atoms are better solvents for this reaction than polar aprotic solvents because polar protic solvents will stabilize anionic intermediate *via* the hydrogen bonding. The outcomes of the solvent screening suggest that $[\text{Fe}_3\text{O}_4@\text{PAM-Schiff base-Mn}][\text{ClO}_4]$ is an enormously effective and convenient catalyst for this Huisgen 1,3-dipolar cycloaddition reaction in ethanol. Under these conditions, the reaction rate increases because the cycloaddition reactions homogeneously occur in the organic phase.



Table 2 Synthesis of β -substituted-1,2,3-triazoles from epoxide or thiiranes in the presence of $[\text{Fe}_3\text{O}_4@\text{PAM-Schiff base-Mn}][\text{ClO}_4]$ MNPs

Entry	Thiiranes/epoxides	Alkyne	Product	Time (min)	Yield ^{a,b} (%)
1		Ph-C≡CH	 1a	15	92
2		Ph-C≡CH	 2a	40	92
3		Ph-C≡CH	 3a	35	89
4		Ph-C≡CH	 4a	35	87
5		Ph-C≡CH	 5a	15	100
6		Ph-C≡CH	 6a	20	97



Table 2 (Contd.)

Entry	Thiiranes/epoxides	Alkyne	Product	Time (min)	Yield ^{a,b} (%)
7		Ph-≡		35	94
8		Ph-≡		30	95
9		Ph-≡		35	93
10		Ph-≡		25	98
11		Ph-≡		25	98
12		Ph-≡		35	95

Table 2 (Contd.)

Entry	Thiiranes/epoxides	Alkyne	Product	Time (min)	Yield ^{a,b} (%)
13				20	99
14				30	97
15				15	100

^a Conditions: epoxide or thiirane (1 mmol), alkyne (1 mmol), sodium azide (1.3 mmol) and $[\text{Fe}_3\text{O}_4@\text{PAM-Schiff base-Mn}][\text{ClO}_4]$ in reflux of ethanol (10 mL). ^b Isolated yields.

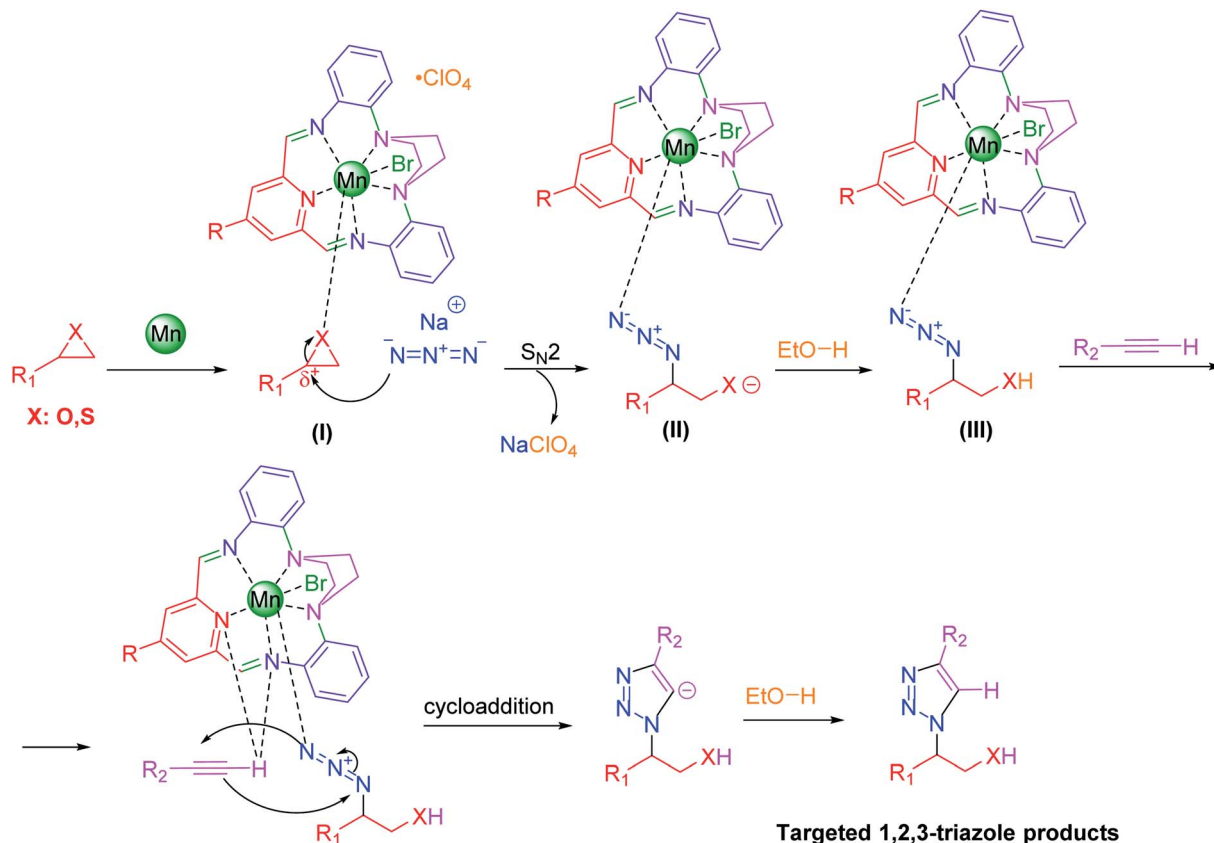
3.2.1.3. Effect of temperature. Furthermore, we optimized the reaction conditions to observe the effect of temperature. In this sense, the reaction was performed at three different temperatures *viz.* 25 °C, 50 °C and 65 °C. There was a drastic decrease in the reaction yield when decreasing the reaction temperature from reflux to 25 °C. Based on the observations, 12 mg of the catalyst in ethanol and at reflux conditions were considered as optimum conditions for the reaction.

3.2.2. Catalyst potential. Therefore, the scope for Huisgen 1,3-dipolar cycloaddition in the synthesis of 1,2,3-triazoles using $[\text{Fe}_3\text{O}_4@\text{PAM-Schiff base-Mn}][\text{ClO}_4]$ catalyst in refluxing of ethanol as the solvent for several substituted three-membered heterocycle (epoxide and thiirane) terminal

alkynes is demonstrated on Table 2. Various 2,3-triazoles adducts were synthesized from the reaction of different substituted epoxides and thiiranes with aliphatic and aromatic terminal alkynes and NaN_3 in high yields without the formation of any by-products. From the experiments it can be concluded that aryl alkynes are much more reactive than aliphatic terminal alkynes. We also demonstrated a gram-scale example – using phenyl acetylene, styrene episulfide and sodium azide – which was obtained in 95% isolated yield.

3.2.3. Reaction mechanism. Based on the literature, the following mechanism for the catalytic synthesis of 1,4-disubstituted-1,2,3-triazoles *via* Huisgen 1,3-dipolar cycloaddition of substituted epoxide, and thiirane with alkynes and NaN_3





Scheme 2 The proposed mechanism for the synthesis of 1,4-disubstituted-1,2,3-triazoles over [Fe₃O₄@PAM-Schiff base-Mn][ClO₄] catalyst.

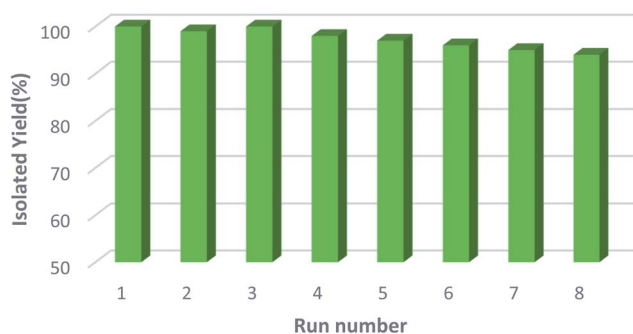


Fig. 10 Reusability of [Fe₃O₄@PAM-Schiff base-Mn][ClO₄] MNPs.

under the catalysis of [Fe₃O₄@PAM-Schiff base-Mn][ClO₄] complex has been illustrated in Scheme 2.

3.2.4. Stability in cyclic test. One of the key benefits of heterogeneous catalyst is the opportunity to reuse it after a simple sequence of filtration/wash and, in some cases, reactivation. Hence, as an added benefit, the recyclability of the [Fe₃O₄@PAM-Schiff base-Mn][ClO₄] catalyst was studied for synthesis of 1,2,3-triazoles for the same reaction several times (Fig. 10). As can be seen, the [Fe₃O₄@PAM-Schiff base-Mn][ClO₄] catalyst can be recycled 8 times without compromising the yield of reactions. These results demonstrate how effective

the Fe₃O₄ can act as a support for Mn-Schiff base complex encapsulation. Even after 8 cycles, the catalyst did not loss activity and its appearance remained the same as depicted in Fig. 10. At the end of each cycle, the catalyst was easily separated from the reaction mixture by magnetic decantation. We also measured the mass balance of the initial and final weight of the catalyst, which reduced by only 2 wt%. It was observed that there was no leaching of Mn from [Fe₃O₄@PAM-Schiff base-Mn][ClO₄] after 8 runs. This reveals that the Mn complex is still bound to the surface of nanomagnetic support and there was really nothing significant on the leaching of Mn after reuse. This provides strong evidence of its structural stability.

3.2.5. Hot-filtration test. The hot filtration test shows that [Fe₃O₄@PAM-Schiff base-Mn][ClO₄] plays an efficient catalytic role in the successful synthesis of the corresponding target molecules without any leaching into the reaction medium.

3.2.6. Comparison. Herein, we aimed at evaluating [Fe₃O₄@PAM-Schiff base-Mn][ClO₄] complex in the synthesis of 1,4-disubstituted-1,2,3-triazoles (Table 3). As depicted in Table 3, the our catalyst is the most efficient catalyst for both of the synthesis of 1,4-disubstituted-1,2,3-triazoles under green conditions. In addition, some of the previously reported catalysts are homogeneous in nature and they cannot be recovered efficiently, so are not environmentally friendly, suffering from various limitations including harsh conditions, hazardous solvents and low yields.

Table 3 Comparison of the synthesis of β -substituted-1,2,3-triazoles in the presence of various catalysts

Entry	Catalyst	Time (min)	Yield ^a (%)	Ref.
1	Nano-MgFe ₂ O ₄ /Cu	300	91	93
2	CuNPs/C	960	76	94
3	Fe ₃ O ₄ @pectin@[(CH ₂) ₃ -acetamide-Cu(II)]	120	97	95
4	Cu ₂ O/rGO(0.5%)/TiO ₂ nanocomposite	120	70	96
5	SiO ₂ /CuSO ₄	360	75	97
6	CuO-NiO	120	84	98
7	CuFe ₂ O ₄ /g-C ₃ N ₄	180	90	99
8	[Fe ₃ O ₄ @PAM-Schiff base-Mn][ClO ₄]	15	92	This work

^a Isolated yields.

4. Conclusion

The Fe₃O₄ supported 5-membered macrocyclic Schiff base proved to be a very efficient solid support for manganese (II) immobilization. A stepwise strategy was efficiently planned by utilization of metal bromide as starting materials, to formation of the macrocycle complex by ring closure reaction and then followed by a salt metathesis reaction to afford the corresponding complex with a bonded bromine ligand in the apical position and a perchlorate counter ion. Morphological analysis demonstrated a well-dispersed encapsulated Mn on the catalyst surface. The catalytic activity results confirmed the excellent activity of the catalyst for cycloaddition reactions. In addition, the recycling tests showed that [Fe₃O₄@PAM-Schiff base-Mn][ClO₄] catalyst could be reused 8 times without losing catalytic efficiency. Our findings contribute to the development of new bio-based materials and the same strategy could be expanded to other industrial relevant metal catalysed reactions.

Conflicts of interest

There are no conflicts to declare.

References

- P. K. Maji, *Curr. Org. Chem.*, 2020, **24**, 1055–1096.
- F. O. Chahkamali, S. Sobhani and J. M. Sansano, *Sci. Rep.*, 2022, **12**, 2867.
- R. K. Ganta, N. Kerru, S. Maddila and S. B. Jonnalagadda, *Molecules*, 2021, **26**, 3270.
- R. Javahershenas, F. M. Arlan, R. H. Prager and J. Khalafy, *ARKIVOC*, 2020, **2020**, 117–152.
- M. O. Rodrigues, M. N. Eberlin and B. A. D. Neto, *Chem. Rec.*, 2021, **21**, 2762–2781.
- L. H. Choudhury and T. Parvin, *Tetrahedron*, 2011, **67**, 8213–8228.
- P. V. Govardhana Reddy, B. Rajendra Prasad Reddy, M. Venkata Krishna Reddy, K. Raghava Reddy, N. P. Shetti, T. A. Saleh and T. M. Aminabhavi, *J. Environ. Manage.*, 2021, **279**, 111603.
- C. S. Graebin, F. V. Ribeiro, K. R. Rogério and A. E. Kummerle, *Curr. Org. Synth.*, 2019, **16**, 855–899.
- S. L. Wang, F. Y. Wu, C. Cheng, G. Zhang, Y. P. Liu, B. Jiang, F. Shi and S. J. Tu, *ACS Comb. Sci.*, 2011, **13**, 135–139.
- H. Yazdani, S. E. Hooshmand and R. S. Varma, *ACS Sustainable Chem. Eng.*, 2021, **9**, 16556–16569.
- L. Reguera and D. G. Rivera, *Chem. Rev.*, 2019, **119**, 9836–9860.
- L. Zeng, B. Huang, Y. Shen and S. Cui, *Org. Lett.*, 2018, **20**, 3460–3464.
- H. Yang, B. Wu, Y. Liu, Z. Wang, M. Xu, T. Yang, Y. Chen, C. Wang and S. Lin, *ACS Omega*, 2019, **4**, 16016–16025.
- S. Shimizu, *Chem. Rev.*, 2017, **117**, 2730–2784.
- K. Li, L. Chen, Y. X. Fan, Y. Wei and S. J. Yan, *J. Org. Chem.*, 2019, **84**, 11971–11982.
- A. Ghatak and M. Das, *ChemistrySelect*, 2021, **6**, 3656–3682.
- M. Monier, A. El-Mekabaty, D. Abdel-Latif, B. Doğru Mert and K. M. Elattar, *Steroids*, 2020, **154**, 108548.
- M. Kazemi and M. Mohammadi, *Appl. Organomet. Chem.*, 2020, **34**, e5400.
- K. M. Elattar, B. D. Mert, M. Monier and A. El-Mekabaty, *RSC Adv.*, 2020, **10**, 15461–15492.
- N. Kaur, N. Ahlawat, P. Bhardwaj, Y. Verma, P. Grewal and N. K. Jangid, *Synth. Commun.*, 2020, **50**, 137–160.
- T. Nagata and Y. Obora, *Asian J. Org. Chem.*, 2020, **9**, 1532–1547.
- G. Surendra Reddy, K. Anebuselvy and D. B. Ramachary, *Chem.-Asian J.*, 2020, **15**, 2960–2983.
- C. Huang, S. Tang, W. Zhang, Y. Tao, C. Lai, X. Li and Q. Yong, *ACS Sustainable Chem. Eng.*, 2018, **6**, 12522–12531.
- R. Singh, H. Kaur and P. Gupta, *Asian J. Chem.*, 2021, **33**, 2896–2918.
- D. Pereira, M. Pinto, M. Correia-Da-silva and H. Cidade, *Molecules*, 2021, **207**, 230.
- J. S. S. Neto and G. Zeni, *Coord. Chem. Rev.*, 2022, **409**, 213217.
- M. Dhameja, H. Kumar and P. Gupta, *Asian J. Org. Chem.*, 2020, **9**, 721–748.
- R. Varala, H. B. Bollikolla and C. M. Kurmarayuni, *Curr. Org. Synth.*, 2021, **18**, 101–124.
- A. Oubella, A.-E. El Mansouri, M. Fawzi, A. Bimoussa, Y. Laamari, A. Auhmani, H. Morjani, A. Robert, A. Riahi and M. Youssef Ait Itto, *Bioorg. Chem.*, 2021, **115**, 105184.
- A. Pawar, S. Gajare, A. Jagdale, S. Patil, W. Chandane, G. Rashinkar and S. Patil, *Catal. Lett.*, 2021, **152**, 1854–1868.



- 31 M. Breugst and H.-U. Reissig, *Angew. Chem., Int. Ed.*, 2020, **59**, 12293–12307.
- 32 V. V. Kouznetsov, L. Y. Vargas-Méndez and F. I. Zubkov, *Mini-Rev. Org. Chem.*, 2016, **13**, 488–503.
- 33 C. Venkata Ramana Reddy and G. Ganga Reddy, *Lett. Org. Chem.*, 2021, **18**, 187–194.
- 34 A. Pucci, G. Albano, M. Pollastrini, A. Lucci, M. Colalillo, F. Oliva, C. Evangelisti, M. Marelli, D. Santalucia and A. Mandoli, *Catalysts*, 2022, **10**, 434.
- 35 M. Srinivas, A. Singh Pathania, P. Mahajan, P. K. Verma, S. S. Chobe, F. A. Malik, A. Nargotra, R. A. Vishwakarma and S. D. Sawant, *Bioorg. Med. Chem. Lett.*, 2018, **28**, 1005–1010.
- 36 V. K. R. Avula, S. Vallela, J. S. Anireddy and N. R. Chamarthi, *J. Heterocycl. Chem.*, 2017, **54**, 3071–3076.
- 37 F. Casti, F. Basoccu, R. Mocci, L. De Luca, A. Porcheddu and F. Cuccu, *Molecules*, 2022, **27**, 1988.
- 38 R. A. Sheldon, M. L. Bode and S. G. Akakios, *Curr. Opin. Green Sustainable Chem.*, 2022, **33**, 100569.
- 39 M. Huerta-Madroñal, J. Caro-León, E. Espinosa-Cano, M. R. Aguilar and B. Vázquez-Lasa, *Carbohydr. Polym.*, 2021, **273**, 118619.
- 40 C. Huang, Y. Su, J. Shi, C. Yuan, S. Zhai and Q. Yong, *New J. Chem.*, 2019, **43**, 3520–3528.
- 41 B. Niknam, F. Haji Aboutaleb, W. Ma and R. Masoudi Nejad, *Structures*, 2021, **34**, 4986–4998.
- 42 W. MA, *Chem. Eng. J.*, 2020, **395**, 1–171.
- 43 S. Kar, H. Sanderson, K. Roy, E. Benfenati and J. Leszczynski, *Chem. Rev.*, 2022, **122**, 3637–3710.
- 44 H. Dong, L. Zheng, P. Yu, Q. Jiang, Y. Wu, C. Huang and B. Yin, *ACS Sustainable Chem. Eng.*, 2020, **8**, 256–266.
- 45 J. Jiang, T. Zhang and D. Chen, *IEEE Trans. Power Electron.*, 2021, **36**, 10214–10223.
- 46 L. Soltys, O. Olkhovyy, T. Tatarchuk and M. Naushad, *Magnetochemistry*, 2021, **7**, 145.
- 47 P. K. P. G. Chopra, T. L. Lambat, S. H. Mahmood, R. G. Chaudhary and S. Banerjee, *ChemistrySelect*, 2021, **6**, 6867–6889.
- 48 C. Grison and Y. Lock Toy Ki, *Curr. Opin. Green Sustainable Chem.*, 2021, **29**, 100461.
- 49 X. Li, Z. Shang, F. Peng, L. Li, Y. Zhao and Z. Liu, *J. Power Sources*, 2021, **512**, 230512.
- 50 S. E. Mudiyansele, P. H. D. Nguyen, M. S. Rajabi and R. Akhavan, *Electron*, 2021, **10**, 2558.
- 51 T. Itoh and Y. Takagi, *ACS Sustainable Chem. Eng.*, 2021, **9**, 1443–1458.
- 52 P. Gómez-López, A. Puente-Santiago, A. Castro-Beltrán, L. A. Santos do Nascimento, A. M. Balu, R. Luque and C. G. Alvarado-Beltrán, *Curr. Opin. Green Sustainable Chem.*, 2020, **24**, 48–55.
- 53 J. Sun, S. Abednatanzi, P. Van Der Voort, Y.-Y. Liu and K. Leus, *Catalysts*, 2020, **10**, 578.
- 54 T. K. Pal, D. De and P. K. Bharadwaj, *Fuel*, 2022, **320**, 123904.
- 55 R. Ghanbarinia Firozjah, A. Sadeghi and S. Khoee, *ACS Omega*, 2020, **5**, 27119–27132.
- 56 Z. Zhang, H. Li, D. Wu, L. Zhang, J. Li, J. Xu, S. Lin, A. K. Datye and H. Xiong, *Coord. Chem. Rev.*, 2022, **460**, 214469.
- 57 J. I. Orege, O. Oderinde, G. A. Kifle, A. A. Ibikunle, S. A. Raheem, O. Ejeromedoghene, E. S. Okeke, O. M. Olukowi, O. B. Orege, E. O. Fagbohun, T. O. Ogundipe, E. P. Avor, O. O. Ajayi and M. O. Daramola, *Energy Convers. Manage.*, 2022, **258**, 115406.
- 58 A. Gopinath, L. Pisharody, A. Popat and P. V. Nidheesh, *Curr. Opin. Solid State Mater. Sci.*, 2022, **26**, 100981.
- 59 Z. Wang, Q. Lei, Z. Wang, H. Yuan, L. Cao, N. Qin, Z. Lu, J. Xiao and J. Liu, *Chem. Eng. J.*, 2020, **395**, 125180.
- 60 J. Min, Z. Xia, T. Zhang, H. Su, Y. Zhi and S. Shan, *Chem. Pap.*, 2021, **75**, 2965–2980.
- 61 M. Bracci, P. C. Bruzzese, A. Famulari, D. Fioco, A. Guidetti, Y.-K. Liao, L. Podvorica, S. F. Rezayi, I. Serra, K. Thangavel and D. M. Murphy, *Electron Paramagn. Reson.*, 2021, **27**, 1–46.
- 62 W.-F. Lai, R. Tang and W.-T. Wong, *Pharmaceutics*, 2020, **12**, 725.
- 63 F. Moccia, L. Rigamonti, A. Messori, V. Zanotti and R. Mazzoni, *Molecules*, 2021, **26**, 2728.
- 64 R. Ahorsu, M. Constanti and F. Medina, *Ind. Eng. Chem. Res.*, 2021, **60**, 18612–18626.
- 65 S. R. Obireddy and W. F. Lai, *Int. J. Nanomed.*, 2022, **17**, 589–601.
- 66 S. Adewale Akintelu, A. Kolawole Oyebamiji, S. Charles Olugboko and D. Felix Latona, *Curr. Res. Green Sustainable Chem.*, 2021, **4**, 100176.
- 67 S. Shylesh, V. Schünemann and W. R. Thiel, *Angew. Chem., Int. Ed.*, 2010, **49**, 3428–3459.
- 68 M. S. Pourbavarsad, B. J. Jalalieh, N. Landes and W. A. Jackson, *J. Environ. Chem. Eng.*, 2022, **10**, 107001.
- 69 C. W. Lim and I. S. Lee, *Nano Today*, 2010, **5**, 412–434.
- 70 C. O. L. Mbuya, L. L. Jewell, T. S. Ntelane and M. S. Scurrall, *Rev. Chem. Eng.*, 2020, DOI: [10.1515/revce-2020-0017](https://doi.org/10.1515/revce-2020-0017).
- 71 F. Zaera, *Chem. Rev.*, 2022, **122**, 8594–8757.
- 72 X.-Y. Li, Q.-P. Kang, C. Liu, Y. Zhang and W.-K. Dong, *New J. Chem.*, 2019, **43**, 4605–4619.
- 73 Y.-X. Sun, Z.-Z. Chen, G. Guo, R.-Y. Li, T. Zhang and W.-K. Dong, *New J. Chem.*, 2021, **45**, 21928–21940.
- 74 L.-M. Pu, X.-X. An, C. Liu, H.-T. Long and L. Zhao, *Appl. Organomet. Chem.*, 2020, **34**, e5980.
- 75 S. G. Saremi, H. Keypour, M. Noroozi and H. Veisi, *RSC Adv.*, 2018, **8**, 3889–3898.
- 76 P. Mahadevi and S. Sumathi, *Synth. Commun.*, 2020, **50**, 2237–2249.
- 77 S. Arulmurugan, H. P. Kavitha and B. R. Venkatraman, *Rasayan J. Chem.*, 2010, **3**, 385–410.
- 78 R. Zhang, Y. Chen, M. Ding and J. Zhao, *Nano Res.*, 2022, **15**, 2810–2833.
- 79 M. Nikoorazm, A. Ghorbani-Choghamarani and N. Noori, *J. Porous Mater.*, 2015, **22**, 877–885.
- 80 A. L. Berhanu, I. Gaurav, I. Mohiuddin, A. K. Malik, J. S. Aulakh, V. Kumar and K.-H. Kim, *TrAC, Trends Anal. Chem.*, 2019, **116**, 74–91.
- 81 S. Protti and M. Fagnoni, *Photochem. Photobiol. Sci.*, 2009, **8**, 1499–1516.



- 82 L. K. Abdul Karem, F. Y. Waddai and N. H. Karam, *J. Pharma Sci. Res.*, 2018, **10**, 1912–1917.
- 83 S. R. Collinson and D. E. Fenton, *Coord. Chem. Rev.*, 1996, **148**, 19–40.
- 84 V. Kandathil, T. S. Koley, K. Manjunatha, R. B. Dateer, R. S. Keri, B. S. Sasidhar, S. A. Patil and S. A. Patil, *Inorg. Chim. Acta*, 2018, **478**, 195–210.
- 85 A. Mohammadi, M. Barikani and M. M. Lakouraj, *Mater. Sci. Eng., C*, 2016, **66**, 106–118.
- 86 H. Yao, Y. Wang and M. K. Razi, *RSC Adv.*, 2021, **11**, 12614–12625.
- 87 A. Mazaheri and M. Bostanian, *Res. Chem. Intermed.*, 2020, **46**, 2327–2350.
- 88 N. Kurnaz Yetim, F. Kurşun Baysak, M. M. Koç and D. Nartop, *J. Mater. Sci.: Mater. Electron.*, 2020, **31**, 18278–18288.
- 89 H. S. Yaddanapudi, K. Tian, S. Teng and A. Tiwari, *Sci. Rep.*, 2016, **6**, 33659.
- 90 F. Laves and H. Wallbaum, *Z. Angew. Mineral.*, 1941, **4**, 17–46.
- 91 L. T. M. Thy, P. M. Cuong, T. H. Tu, H. M. Nam, N. H. Hieu and M. T. Phong, *Chem. Eng. Trans.*, 2020, **78**, 277–282.
- 92 B. Maleki, O. Reiser, E. Esmailnezhad and H. J. Choi, *Polyhedron*, 2019, **162**, 129–141.
- 93 V. R. Velpuri and K. Muralidharan, *J. Organomet. Chem.*, 2019, **884**, 59–65.
- 94 F. Alonso, Y. Moglie, G. Radivoy and M. Yus, *J. Org. Chem.*, 2011, **76**, 8394–8405.
- 95 H. Khashei Siuki, P. Ghamari Kargar and G. Bagherzade, *Sci. Rep.*, 2022, **12**, 3771.
- 96 M. Mirza-Aghayan, M. Saeedi and R. Boukherroub, *Appl. Organomet. Chem.*, 2020, **34**, e5928.
- 97 M. Ciyabi Hashjin, R. Ciyabi, M. Baharloui, G. Hosseini and H. Tavakoli, *Chin. J. Chem.*, 2012, **30**, 223–227.
- 98 S. Gajurel, B. Dam, M. Bhushan, L. R. Singh and A. K. Pal, *Appl. Organomet. Chem.*, 2022, **36**, e6524.
- 99 D. Khalili and M. Rezaee, *Appl. Organomet. Chem.*, 2019, **33**, e5219.

